

## Spin-Dependent Electron Transport in Manganite Bicrystal Junctions

A. M. Petrzhhik<sup>a,\*</sup>, V. V. Demidov<sup>a</sup>, G. A. Ovsyannikov<sup>a,b</sup>, I. V. Borisenko<sup>a</sup>, and A. V. Shadrin<sup>a,b</sup>

<sup>a</sup>*Kotel'nikov Institute of Radio Engineering and Electronics, Russian Academy of Sciences,  
Mokhovaya ul. 11, Moscow, 125009 Russia*

<sup>b</sup>*Chalmers University of Technology, SE-41296, Gothenburg, Sweden*

\*e-mail: petrzhhik@hitech.cplire.ru

Received December 31, 2011

**Abstract**—Magnetic bicrystal films and junctions of magnetic  $\text{La}_{0.67}\text{Sr}_{0.33}\text{MnO}_3$  (LSMO) and  $\text{La}_{0.67}\text{Ca}_{0.33}\text{MnO}_3$  (LCMO) films epitaxially grown on  $\text{NdGaO}_3$  substrates with the (110) planes of their two parts misoriented (tilted) at angles of  $12^\circ$ ,  $22^\circ$ ,  $28^\circ$ , and  $38^\circ$  are investigated. For comparison, bicrystal boundaries with a  $90^\circ$  misorientation of the axes of the  $\text{NdGaO}_3$  (110) planes were fabricated. The directions of the axes and the magnetic anisotropy constants of the films on both sides of the boundary are determined by two independent techniques of magnetic resonance spectroscopy. The magnetic misorientation of the axes in the substrate plane has been found to be much smaller than the crystallographic misorientation for tilted bicrystal boundaries, while the crystallographic and magnetic misorientation angles coincide for boundaries with rotation of the axes. An increase in the magnetoresistance and characteristic resistance of bicrystal junctions with increasing misorientation angle was observed experimentally. The magnetoresistance of bicrystal junctions has been calculated by taking into account the uniaxial anisotropy, which has allowed the contributions from the tunneling and anisotropic magnetoresistances to be separated. The largest tunneling magnetoresistance was observed on LCMO bicrystal junctions, in which the characteristic resistance of the boundary is higher than that in LSMO boundaries.

DOI: 10.1134/S1063776112100093

### 1. INTRODUCTION

Magnetic junctions are a basic element of spintronic devices, where the manipulations are made not with the system's charge state but with its spin state [1]. Ferromagnets with a spin polarization of carriers close to 100% are the most attractive materials for use in magnetic junctions. When such materials are used in magnetic junctions, one may expect record magnetoresistances and observe the strongest effects caused by strong spin injection (see, e.g., [2]).

Doped  $\text{La}_{1-x}\text{A}_x\text{MnO}_3$  (where  $\text{A} = \text{Sr}, \text{Ca}, \text{Ba}, \dots$ ) manganites at an optimal doping level  $x \approx 0.33$  are ferromagnetic materials with a high polarization of carriers close to 100% (see, e.g., [3]). In the ferromagnetic state, these materials are semimetal ferromagnets in which the electron density of states at the Fermi level is completely spin-polarized, so that the conductivity is governed mainly by spin-polarized carriers [4]. Films fabricated from such materials are most attractive from the viewpoint of applications. A large number of works on the magnetoresistance in manganite films, as a rule, grown on  $\text{SrTiO}_3$  (STO) substrates are known [5–15]. In addition to studying the low-field anisotropy of films, the magnetic junctions in such films are studied in a number of papers. The creation of magnetic junctions from manganites is complicated by their high sensitivity to both degradation of the

chemical composition and change of the electronic state near the bicrystal boundary. One way to produce magnetic junctions is to create a bicrystal boundary in a thin epitaxial film by epitaxial growth of a film on a substrate consisting of two misoriented single-crystal pieces. In recent years, much attention has been given to studying manganite junctions at bicrystal boundaries produced in epitaxial films grown on STO bicrystal substrates with rotation of the crystallographic axes of manganites around the normal to the substrate plane (rotated bicrystal (RB) junctions) [16–18].

The magnetoresistance is traditionally defined as  $\text{MR} = (R_1 - R_0)/R_0$ , where  $R_0$  is the resistance in zero magnetic field ( $H = 0$ ) and  $R_1$  is the resistance at  $H \neq 0$ . The magnetoresistance depends on the magnetic field. However, in several cases, for example, for the tunneling and anisotropic magnetoresistances, to operate not the function but a specific value, it is convenient to define the low-field tunneling magnetoresistance as  $\text{MR} = (R_{\text{max}} - R_0)/R_0$ . Here,  $R_{\text{max}}$  is the maximum resistance. A large number of works on the magnetoresistance in manganite films, as a rule, grown on STO substrates are known [5–15]. The produced bicrystal junctions had a tunneling magnetoresistance of several tens of percent at fields below 1 kOe and a characteristic resistance varying in a wide range, depending on the quality of the bicrystal substrate

boundary ( $10^{-7}$ – $10^{-5}$   $\Omega$  cm<sup>2</sup>). After annealing, the tunneling magnetoresistance increased to 300% [19]. Its value also grew with increasing misorientation angle from zero to 45° [20]. At such a high tunneling magnetoresistance, the contributions from the colossal and anisotropic magnetoresistances of the manganite films may be neglected, because they are small compared to the tunneling one. As previous studies of bicrystal boundaries of cuprate semiconductors [18, 19] showed, by rotating the basal planes around the bicrystal boundary line (tilted bicrystal (TB) junctions), the microstructure of the boundary can be improved significantly compared to RB junctions and its faceting can be reduced. This type of bicrystal boundary has a low density of dislocations in the boundary plane and a better boundary morphology [21]. The first experiments carried out on TB junctions showed high tunneling magnetoresistances (up to 150%) for  $\text{La}_{0.67}\text{Ca}_{0.33}\text{MnO}_3$  TB junctions with a rather large resistance of the bicrystal boundary ( $3$ – $5 \times 10^{-5}$   $\Omega$  cm<sup>2</sup>) [22]. At the same time, the tunneling magnetoresistance for  $\text{La}_{1-x}\text{Sr}_x\text{MnO}_3$  TB junctions was several percent and was comparable to the contribution from the anisotropic magnetoresistance [23].

The goal of this paper is to study the magnetic parameters of manganite bicrystal films and the magnetoresistances of  $\text{La}_{0.67}\text{Sr}_{0.33}\text{MnO}_3$  (LSMO) and  $\text{La}_{0.67}\text{Ca}_{0.33}\text{MnO}_3$  (LCMO) bicrystal junctions on NGO substrates with TB misorientation and to compare the results with those for RB misorientation. We also study the contributions from the colossal and anisotropic magnetoresistances of films to the total magnetoresistance of bicrystal junctions.

## 2. SAMPLE FABRICATION AND EXPERIMENTAL TECHNIQUE

Epitaxial LSMO and LCMO films 50–70 nm in thickness were grown by laser ablation on symmetric bicrystal  $\text{NdGaO}_3$  (NGO) substrates with rotation of the (110) NGO planes around the  $[1\bar{1}0]$  NGO direction through angles  $2\theta = 12^\circ, 22^\circ, 28^\circ,$  and  $38^\circ$  (TB junctions, see Fig. 1). Bicrystal substrates with a  $90^\circ$  misorientation were produced by rotating the axes of the (110) NGO plane around the normal to the substrate (RB junctions).

The films were grown in an oxygen atmosphere with a pressure  $P = 0.2$  mbar at a substrate temperature  $T = 750^\circ\text{C}$  followed by cooling in oxygen at a pressure of 1 bar [23, 24]. When the manganite films were grown on NGO substrates, the same epitaxial relationships held for both LSMO and LCMO films. For example, for the LSMO films we have

$$(001)\text{LSMO} \parallel (110)\text{NGO},$$

$$[100]\text{LSMO} \parallel [1\bar{1}0]\text{NGO}.$$

The pseudo-cubic lattice constant is  $a_L = 0.388$  nm for LSMO ( $a_L = 0.3858$  nm for LCMO), while the lattice

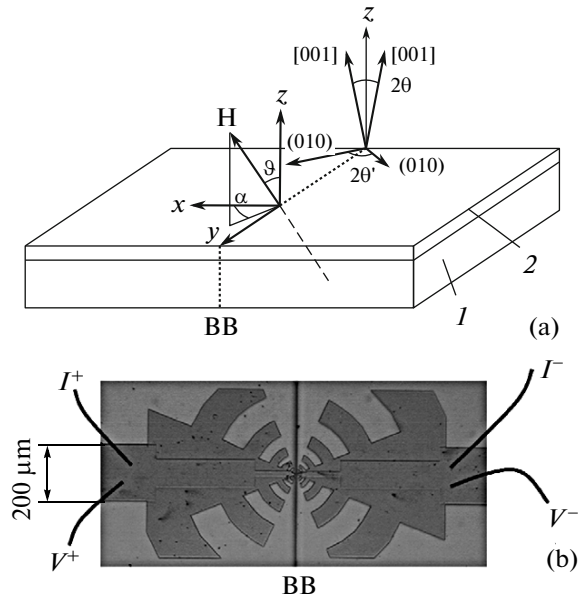


**Fig. 1.** (a) Schematic view of a tilted bicrystal boundary (BB) in manganite film 2 and  $\text{NdGaO}_3$  substrate 1. The crystallographic [001] directions of the two halves of the manganite film for TB junctions are indicated by the arrows. The misoriented (010) planes are also indicated by the arrows RB junctions. The misorientation angles for TB ( $2\theta$ ) and RB ( $2\theta'$ ) junctions are marked. The angles  $\alpha$  and  $\theta$  specifying the external magnetic field direction are shown. The  $x$  and  $y$  axes coincide with the current direction and the bicrystal boundary, respectively. (b) A photo of a bicrystal junction connected to a logoperiodic antenna. The lead lines for a four-point junction resistance measurement are shown schematically.

constants for (110) NGO (an orthorhombic cell,  $a = 0.5426$  nm,  $b = 0.5502$  nm,  $c = 0.7706$  nm) along the [001] and  $[1\bar{1}0]$  directions are  $a_N = 0.3853$  nm and  $b_N = 0.3863$  nm, respectively [25, 26]. During epitaxial growth, nonuniform compression is observed in the substrate plane in LSMO films [24, 25]. Heteropolar mechanical strains arise in LCMO films, compressive along the [001] NGO direction and tensile along the  $[1\bar{1}0]$  NGO direction, because  $a_N < a_L < b_N$ . During epitaxial growth, the crystal structure of the bicrystal substrate is repeated in the manganite film and a bicrystal boundary is formed in the film.

Bridges 6–8  $\mu\text{m}$  in width crossing the bicrystal boundary were formed by ion-beam etching using a photoresist mask (see the central part of Fig. 1b). All electrophysical measurements were made by a four-point method using platinum or gold contact pads. A dc current flowed in the film plane perpendicular to the boundary, and the direction of the external magnetic field was varied and was specified by two angles: the polar  $\alpha$  and azimuthal  $\theta$  (see Fig. 1a).

To determine the magnetic anisotropy parameters, we applied two independent techniques based on the resonance absorption of electromagnetic radiation by

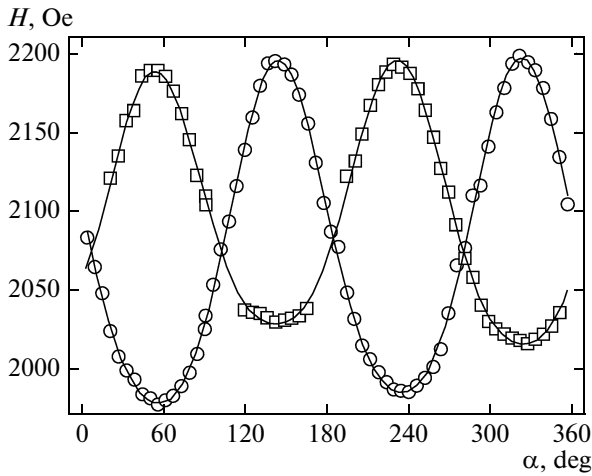


**Fig. 2.** Angular dependences of the resonance fields for two FMR lines in an LSMO film.

ferromagnetic films. First, we used a standard X-band (a frequency  $\sim 10$  GHz) Bruker ER-200 EPR spectrometer to take the angular dependences of the ferromagnetic resonance (FMR) spectra in the so-called parallel orientation. In this case, the samples were rotated through  $360^\circ$  around an axis perpendicular to the substrate plane, while the dc magnetic field and the magnetic component of the microwave field were always mutually perpendicular and remained in the film plane. This technique allows both the directions of the magnetic anisotropy axes and the anisotropy constants to be determined with a good accuracy [24].

However, the spin-dependent transport in manganese bicrystal junctions suggests using much weaker external magnetic fields than those required for the X-band FMR spectra to be observed (about 2 kOe). Therefore, we also used the second technique based on a sharp increase in the dc magnetic susceptibility of a uniaxial ferromagnet for an external magnetic field direction along the hard magnetization axis [24, 27] under conditions where the field strength is varied near the uniaxial anisotropy field. To implement the second technique, we used a homemade magnetic resonance spectrometer whose operation is based on a Q-meter [28]. The angular dependences of the absorption spectra were also taken under parallel orientation conditions. The external magnetic field was varied in the range from  $-300$  to  $300$  Oe. When its direction approached the direction of the hard magnetization axis of uniaxial magnetic anisotropy, the electromagnetic radiation absorption signal increased sharply in the range of values equal to the uniaxial anisotropy field strength.

### 3. FERROMAGNETIC RESONANCE IN BICRYSTAL JUNCTIONS

The angular dependences of the FMR spectra were studied at room temperature. Complex spectral curves were generally observed when FMR was recorded on manganite films grown on bicrystal substrates. Nevertheless, we always managed to identify the main doublet of lines and to trace their evolution during the sample rotation. Figure 2 shows an example of the angular dependence of the resonance fields for the FMR lines corresponding to the two parts of the LSMO film separated by the bicrystal boundary produced by a  $90^\circ$  RB misorientation of the NGO substrate.

First of all, it should be noted that the uniaxial (with  $\pi$  periodicity) magnetic anisotropy dominates over the cubic (with  $\pi/2$  periodicity) one. This is typical of manganite films grown on NGO substrates [11–13, 24, 25, 29]. In addition, Fig. 2 shows that we failed to separately identify the lines (there are no experimental points) for certain angles  $\alpha$ . At the same time, we can assert with confidence that the easy axes of uniaxial magnetic anisotropy from the film areas on different sides of the boundary are misoriented at an angle close to  $90^\circ$ . The relation between the electromagnetic radiation frequency and FMR magnetic field  $H$  can be derived in analytical form with an explicit dependence on the sought-for anisotropy parameters [24]:

$$\left(\frac{\omega}{\gamma}\right)^2 = \left(4\pi M_0 + H_0 + \frac{2K_u}{M_0} \cos^2 \varphi_u + \frac{2K_c}{M_0} \frac{1 + \cos^2 2\varphi_c}{2}\right) \times \left(H_0 + \frac{2K_u}{M_0} \cos^2 \varphi_u + \frac{2K_c}{M_0} \cos 4\varphi_c\right). \quad (1)$$

Here,  $\omega$  is the angular frequency,  $\gamma$  is the gyromagnetic ratio,  $M_0$  is the equilibrium magnetization,  $\varphi_u$  and  $\varphi_c$  are the angles between the external magnetic field and the easy axes of uniaxial and cubic (crystallographic) anisotropies, respectively, and  $K_u$  and  $K_c$  are the uniaxial and cubic anisotropy constants. In turn, these constants specify the uniaxial,  $H_u = 2K_u/M_0$ , and cubic,  $H_c = 2K_c/M_0$ , anisotropy fields. Thus, the technique based on the FMR spectra gives sufficient information about the anisotropy parameters of the objects under study (Table 1).

From the data in Table 1, it can be concluded that the misorientation of the easy axes of uniaxial magnetic anisotropy is in the range  $4^\circ$ – $90^\circ$  and depends on both misorientation angle and type for the two parts of the bicrystal substrate. It follows from the results of [26] that cube-on-cube growth is observed when LSMO films are grown on the (110) NGO plane. Our magnetic measurements [24, 25] and those in [12] showed that the easy axis of the LSMO film deposited

**Table 1.** Magnetic anisotropy parameters for LSMO bicrystal films and junctions determined by two independent techniques at  $T = 300$  K

Sample number	$2\theta$ , deg	$2\theta'$ , deg	$H_u$ , Oe	$\alpha_{\text{easy}}$ , deg	$\alpha_{\text{hard}}$ , deg	$\Delta\alpha$ , deg	Sample type
817	0	90	123 98.4	53.8 -37.6	146.4 54.3	91.4–92.1	film
866	12	0	90 137	–	89.4 90.6	1.2	junctions
843	0	90	154 248	48.7 -40.9	-47.4 44.0	89.6–91.4	junctions

Note:  $2\theta$  is the misorientation angle of the crystallographic (001) LSMO planes,  $2\theta'$  is the misorientation angle of the [010] LSMO directions,  $H_u$  is the uniaxial magnetic anisotropy field,  $\alpha_{\text{easy}}$  is the deflection angle of the easy magnetization axis of LSMO measured from the normal to the bicrystal boundary obtained by the X-band FMR technique,  $\alpha_{\text{hard}}$  is the deflection angle of the hard magnetization axis obtained by the microwave absorption technique at 300 MHz, and  $\Delta\alpha$  is the misorientation angle of the magnetizations in the substrate plane.

on the (110) NGO plane coincides with the  $[1\bar{1}0]$  NGO direction. As a result, for bicrystal films with RB boundaries and a misorientation angle of the  $[1\bar{1}0]$  NGO axes  $2\theta' = 90^\circ$ , the directions of the easy axes should differ by  $90^\circ$ . In our experiment, the misorientation of the magnetization axes is in the range  $89^\circ$ – $92^\circ$ . In symmetric bicrystal RB films, misorientation of the easy magnetization axes is also observed in the substrate plane, but it is much smaller than that of the (110) NGO planes [12, 24, 25]. It may well be that the tilt of the (110) NGO plane changes the magnetic anisotropy of the LSMO film [24]. A similar misorientation of the axes was observed in LSMO films on bicrystal substrates [18].

Figure 3 shows an example of the angular dependence of the absorption signal of electromagnetic radiation at room temperature with a frequency of 300 MHz for an LSMO bicrystal film with a misorientation angle of  $90^\circ$  as the external magnetic field is varied. To simplify the figure, only the positive range of external magnetic fields is shown. Changing the magnetic field in the opposite direction leads to similar dependences.

Above, it has already been noted that all measurements based on this technique were made in the same range of external magnetic fields at which the magnetoresistance of bicrystal junctions was investigated. In addition, the narrowness of the absorption lines depending on both misorientation angle (see the inset in Fig. 3) and external magnetic field strength allows the signals from the two parts of the bicrystal film to be separated more reliably in some cases (in particular, for the same direction of the magnetization axes). This is particularly important for small misorientation angles of the crystallographic axes of the substrate, when the relatively large FMR widths do not allow the resonance lines from the two parts of the film on different sides of the bicrystal boundary to be separated.

It can be clearly seen from Fig. 3 that there are two types of absorption lines that should be attributed to the two parts of the bicrystal film. Numerical calculations in the model of a uniaxial ferromagnet in a similar geometry indicate that the angles corresponding to the resonances when the angle is varied specify the directions of the hard magnetization axes, while the magnetic field strengths corresponding to the peaks when  $H$  is varied give the uniaxial anisotropy fields. Given that the hard and easy magnetization axes in a uniaxial ferromagnet are perpendicular to each other, both techniques yielded similar values for the magnetic anisotropy parameters of the investigated bicrystal films (see Table 1). The deviation of the difference between the measured angles of the anisotropy axes from  $90^\circ$  for RB boundaries is due to the inaccuracy (a few degrees) of the original sample installation on the holder. Note that the presence of a cubic magnetic anisotropy component in the samples shifts the real peaks. However, first, this shift is negligible for films

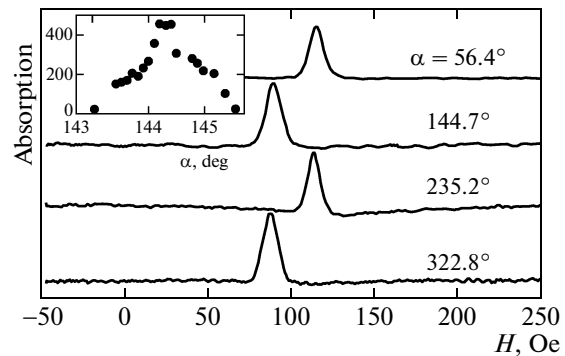


**Fig. 3.** Field dependences of the absorption signals at 300 MHz for a bicrystal film with an RB misorientation angle  $2\theta' = 90^\circ$  at various angles  $\alpha$  between the external magnetic field and the  $x$  axis. The inset shows the angular dependence of the amplitude of the absorption peak (in rel. units) near  $\alpha = 144^\circ$ .

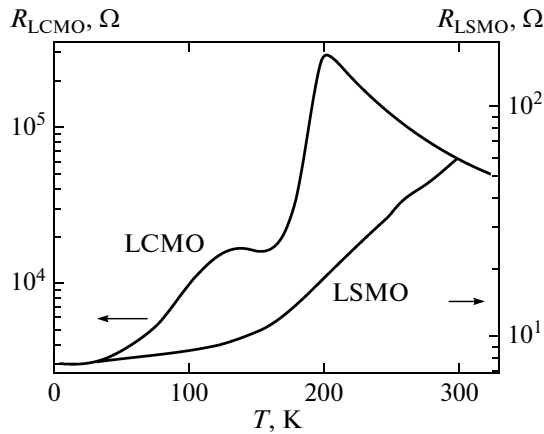


**Fig. 4.** Temperature dependences of the resistance for manganite bicrystal junctions on LSMO RB ( $2\theta' = 90^\circ$ ) and LCMO TB ( $2\theta = 28^\circ$ ) films. The measurements were made in the Earth's magnetic field ( $H \approx 0.5$  Oe).

grown on NGO substrates and, second, it can be easily taken into account in numerical calculations.

It should be noted that the measured absorption is due to the imaginary part of the dynamic magnetic susceptibility. The latter, in turn, is the product of the static magnetic susceptibility, whose resonant behavior is used in the technique under consideration, and a function dependent on the relaxation time  $\tau$  and defining the magnetization decay. This function has a maximum at  $\omega\tau = 1$ . In the films being investigated, these times presumably lie in the range  $10^{-9}$ – $10^{-8}$  s, which determined the choice of the frequency for the second technique. This technique allows  $\tau$  in uniaxial ferromagnets to be obtained in principle when the absorption spectra are taken at different frequencies. A signal of the same nature was also observed at 10 GHz, but its amplitude was much smaller, which did not allow the required sensitivity to be achieved.

#### 4. MAGNETORESISTANCE OF BICRYSTAL BRIDGE JUNCTIONS

##### 4.1. Temperature Dependences

Figure 4 shows the temperature dependences of the resistance for LCMO and LSMO bicrystal bridge junctions produced in the absence of an external magnetic field.

The transition of manganites to a ferromagnetic state near the Curie temperature  $T_C$  is generally accompanied by an insulator–metal transition, which manifests itself as a peak in the temperature dependence of the resistance at  $T_p$ .  $T_p$  and  $T_C$  usually coincide to within a few degrees [12, 30]. The Curie temperature for epitaxial LCMO and LSMO films was determined from the temperature dependence of the electron magnetic resonance field using the technique described in detail in [24, 25]. As can be seen from Fig. 4, for the bicrystal junctions under consideration,

$T_p$  is 210 K for LCMO and more than 300 K for LSMO. Comparison of the temperature dependences of the resistance for LCMO bicrystal junctions and an epitaxial film bridge shows that near the boundary  $T_p$  decreases to 130 K compared to  $T_p = 210$  K in the films forming the bicrystal boundary. This manifests itself most clearly when the resistance of the lead bicrystal junction films is taken into account [26, 31].

The high characteristic resistance of the LCMO junction,  $RA = 10^{-7}$ – $10^{-5}$   $\Omega$  cm<sup>2</sup> (where  $R$  and  $A$  are the resistance and cross-sectional area of the bicrystal junction, respectively), at  $T = 4.2$  K suggests the presence of a barrier layer with a transparency of  $10^{-4}$ – $10^{-3}$  (determined by the parameter  $RA$ ). A dramatic decrease in charge density to its critical value at which a ferromagnetic material with a reduced temperature  $T_C$  is formed is most likely responsible for the appearance of such a barrier. In LSMO bicrystal junctions, no clear second peak is observed in the dependence  $R(T)$ . This suggests a negligible contribution from the transition layer with suppressed ferromagnetism near the bicrystal boundary, while the lower (than for LCMO) characteristic resistance of LSMO junctions,  $RA = 10^{-7}$ – $10^{-5}$   $\Omega$  cm<sup>2</sup>, indicates that the transparency of the barrier layer is higher than that of LCMO junctions. Nevertheless, it should be noted that more detailed measurements of the temperature dependence of the resistance for RB junctions on STO [20] revealed a boundary layer with a reduced Curie temperature ( $T_p \approx 250$  K) in LSMO.

##### 4.2. Dependence of the Magnetoresistance of Bicrystal Junctions on External Magnetic Field

Figure 5 shows the field dependences of the magnetoresistance of an LSMO bicrystal junction with a misorientation angle  $2\theta = 12^\circ$  for three directions of the magnetic field ( $\alpha = 5^\circ, 51^\circ, 85^\circ$ ) lying in the substrate plane ( $\vartheta = 90^\circ$ ) at  $T = 77$  K. The magnetoresistance was normalized to the junction resistance at an external magnetic field  $H = 1$  kOe.

It can be seen from Fig. 5 that the resistance decreases with increasing field at fairly large external magnetic field strengths. Such a decrease is commonly explained by the presence of colossal magnetoresistance in these materials [5, 6, 9], which is decisive in strong magnetic fields ( $\sim 10$  kOe).

In weak magnetic fields (several hundred Oe), a magnetic field hysteresis typical of ferromagnets is observed (see Fig. 5). In the case of coincidence between the directions of the external magnetic field and the passing current, maximal positive bell-shaped resistance peaks were observed. These can be explained both by the tunneling magnetoresistance when the current passes through the boundary [32] and by the anisotropic magnetoresistance of the film itself. The latter can be caused by anisotropy in the spin–orbit interaction between the  $e_{g\uparrow}$  and  $e_{2g\uparrow}$  orbitals of manganese ions [7, 14], the scattering of spin-

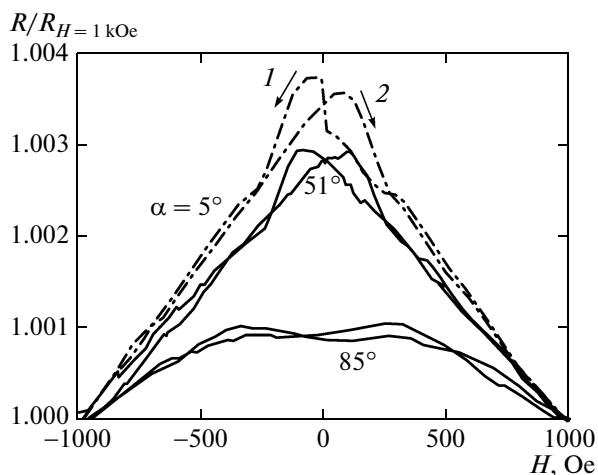


**Fig. 5.** Magnetoresistance of an LSMO bicrystal junction with a misorientation angle  $2\theta = 12^\circ$  at  $T = 77$  K for various external magnetic field directions:  $\alpha = 5^\circ$ ,  $51^\circ$ , and  $85^\circ$ ; the angle  $\theta = 90^\circ$  did not change. The arrows indicate the direction of the change in external magnetic field.

polarized electrons when passing through moving magnetic domain walls [33–36], the Hall effect [37, 38], and other mechanisms. In our case, the maximum magnetoresistance was observed at  $\alpha = 5^\circ$  and was 0.05%. When the magnetic field direction deflected from the direction of the current, the magnetoresistance decreased.

Figure 6 shows the field dependence of the magnetoresistance of an LCMO bicrystal junction with a misorientation angle  $2\theta = 28^\circ$  at a temperature of 4.2 K. In this case, the external magnetic field was directed along the normal to the film (along the  $z$  axis, see Fig. 1). The effect for the LCMO film is seen to be much larger. The maximum magnetoresistance was about 150%, which corresponds to the record values for LCMO bicrystal junctions [19].

Figure 7 shows the magnetoresistance variation for an LSMO bicrystal junction with a TB misorientation angle  $2\theta = 12^\circ$  for an external magnetic field direction parallel to the electric current ( $\vartheta = 0$ ,  $\alpha = 90^\circ$ , see Fig. 1) and a temperature  $T = 4.2$  K. The external magnetic field was changed many times in the  $\pm 1.3$  kOe range. In our case, two positive magnetoresistance peaks symmetric relative to the zero field are observed. This directly points to the contribution from both the boundary (tunneling magnetoresistance) and the film itself (anisotropic magnetoresistance) to the magnetoresistance. The derived maximum value of  $MR \approx 0.1\%$  is close to the values reached on epitaxial LSMO films [8]. Table 2 presents the magnetoresistances at low temperatures for the investigated bridge junctions. The characteristic resistance  $RA$  and magnetoresistance tend to increase with increasing misorientation angle. Such an increase was observed when the misorientation angle was varied in the range  $4^\circ$ – $40^\circ$  on LSMO films grown on STO bicrystal TB sub-

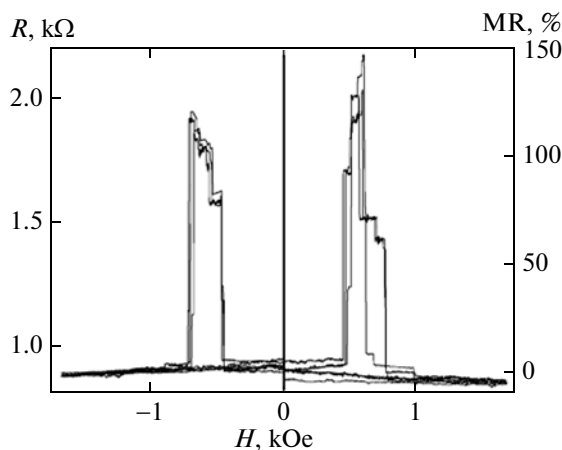


**Fig. 6.** Magnetoresistance of an LCMO bicrystal TB junction with  $2\theta = 28^\circ$  at  $T = 4.2$  K; the external magnetic field is directed along the  $z$  axis.

strates [20]. An increase in  $RA$  is also observed. Sample 905 ( $2\theta = 22^\circ$ ) is disregarded in the dependence of  $RA$  and magnetoresistance on misorientation angle due to the presence of a large number of defects in the bicrystal boundary of the substrate observed through an optical microscope.

To quantitatively describe the tunneling magnetoresistance in magnetic junctions, we used the approach proposed in [39]. In fact, the tunneling conductance between two ferromagnetic media with spin-polarized carriers separated by tunneling barriers should be considered. It should be taken into account that the magnetizations on both sides of the barrier are directed at different angles  $\beta_1$  and  $\beta_2$  relative to the

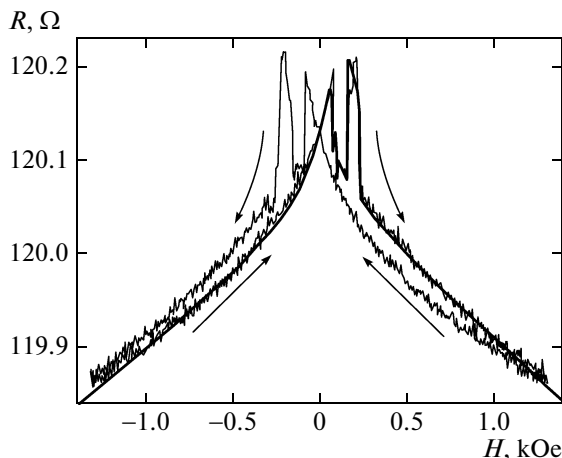


**Fig. 7.** Magnetoresistance of an LSMO bicrystal junction with  $2\theta = 12^\circ$  (sample 866, see Table 1) at  $T = 4.2$  K; the magnetic field is parallel to the flowing current. The arrows indicate the direction of the change in external magnetic field. The results of calculation (thick line) are shown only for a field increasing from  $-1300$  to  $1300$  Oe.

**Table 2.** Magnetoresistance of bicrystal junctions at low temperatures

Sample number	$2\theta$ , deg	$2\theta'$ , deg	Material	$RA$ , $\Omega$ cm <sup>2</sup>	$\alpha$ , deg	$\vartheta$ , deg	MR, %	$H_{\max}$ , Oe
865	0	90	LSMO	$7 \times 10^{-8}$	0	90	0.04	240
843	0	90	LSMO	$2.9 \times 10^{-7}$	0	90	0.015	180
866	12	0	LSMO	$1.2 \times 10^{-6}$	0	90	0.07	200
905	22	0	LSMO	$1.3 \times 10^{-5}$	0	90	0.0017	140
5	28	0	LCMO	$3 \times 10^{-5}$	—	0	150	600
904	38	0	LSMO	$8 \times 10^{-6}$	0	90	6.57	262

Note: MR is the magnetoresistance;  $H_{\max}$  is the magnetic field for which a local resistance peak is observed;  $RA$  is the product of the junction resistance by its area; the designations for the angles  $\alpha$  and  $\vartheta$  are given in Fig. 1;  $2\theta$  and  $2\theta'$  are the misorientation angles; the measurement temperature is  $T = 4.2$  K

boundary. The analytical expression for the spin conductivity  $G_{sp}$  in this situation is [40, 41]

$$G_{sp} = G_{sp}^0 [1 + P^2 \cos(\beta_1 - \beta_2)]. \quad (2)$$

Here,  $G_{sp}^0$  is the conductivity of polarized spins directed at  $90^\circ$  to each other and  $P$  is the polarization of these spins. Taking into account, for completeness, the contribution of nonpolarized carriers,  $G_{ns}$ , to the conductivity, we can write the following expression for the tunneling barrier resistance  $R_{\text{TMR}}$  [39]:

$$R_{\text{TMR}} = \frac{1}{G_{sp} + G_{ns}} = \frac{R_{sp}}{1 + P^2 \cos(\beta_1 - \beta_2) + g}, \quad (3)$$

where  $R_{sp} = 1/G_{sp}$  and  $g \equiv G_{ns}/G_{sp}$ .

The following formula is used to describe the anisotropic magnetoresistance  $R_{\text{AMR}}$  in ferromagnets:

$$R_{\text{AMR}}(\alpha_M) = R_{\perp} + (R_{\parallel} - R_{\perp}) \cos^2 \alpha_M, \quad (4)$$

where  $R_{\perp}$  and  $R_{\parallel}$  are the resistances measured for currents flowing perpendicular and along the magnetization, respectively, and  $\alpha_M$  is the angle between the magnetization and current, which coincides with the angle  $\alpha$  between the magnetic field and current for strong magnetic fields. In [15], dependence (4) was generalized through the phenomenological introduction of a fourth-order tensor for the resistance, which made it possible to take into account the crystallographic symmetry of the samples.

To explain the observed field dependence of the magnetoresistance, both tunneling and anisotropic magnetoresistances should be taken into account simultaneously. For a magnetic field direction perpendicular to the boundary (these are the conditions of the experiment whose results are shown in Fig. 7), the coherent rotation of the magnetizations on both sides of the boundary plays a crucial role in the magnetoresistance of the bridge crossing the boundary [9, 39]. Therefore, we will use dependence (3). However, it should be taken into account that, apart from the bridge itself, the lead areas of the film also contribute to the resistance (see Fig. 1). We will associate their

resistance with the anisotropic magnetoresistance, for which Eq. (4) should be applied. Thus, our numerical analysis of the experimental data was performed using the formula

$$R = R_1^{\perp} + (R_1^{\parallel} - R_1^{\perp}) \cos^2 \alpha_1 + \frac{R_{sp}}{1 + P^2 \cos(\theta_1 - \theta_2) + g} + R_2^{\perp} + (R_2^{\parallel} - R_2^{\perp}) \cos^2 \alpha_2. \quad (5)$$

Here, the subscripts 1 and 2 refer to the two parts of the film on different sides of the boundary. The angles  $\alpha_{1,2}$  and  $\theta_{1,2}$  are specified by the directions of the magnetizations in both parts of the film. These directions were determined for each magnetic field strength from the minimum condition for the free energy

$$F = -(\mathbf{M} \cdot \mathbf{H}) - \frac{K_u}{M^2} (\mathbf{M} \cdot \mathbf{n}_u)^2 + \frac{1}{2} (\mathbf{M} \cdot \hat{N}^c \cdot \mathbf{M}), \quad (6)$$

which takes into account the Zeeman interaction (first term), the induced uniaxial magnetic anisotropy (second term), and the cubic magnetic anisotropy (third term) determined by the LSMO material structure. In Eq. (6),  $\mathbf{M}$  is the magnetic moment vector,  $\mathbf{H}$  is the external magnetic field strength,  $K_u$  is the magnetic anisotropy constant,  $\mathbf{n}_u$  is a unit vector directed along the easy magnetization axis, and  $\hat{N}^c$  is the crystallographic (in our case, cubic) anisotropy tensor. The magnetic moment, the directions of the axes, and the magnetic anisotropy required for this procedure were found by analyzing the magnetic-resonance studies of bicrystal junctions [24].

We performed the calculations numerically and used the magnetization directions found for each magnetic field strength to calculate the field dependence of the junction resistance from Eq. (5) by adding the linear (in field) dependence due to the colossal magnetoresistance effect. To obtain the curve describing the experimental results in Fig. 7, we used the directions of the hard magnetization axes derived from our magnetic-resonance measurements at 300 MHz

and given in Table 1 (see the fifth column for sample 866). Unfortunately, the angular dependence of FMR does not allow us to separate the spectra from the parts located on different sides of the boundary due to the small misorientation of the magnetization axes (see the caption to Fig. 3). As regards the numerical values for the anisotropy fields, in the term describing the anomalous magnetoresistance we took the values from Table 1 (see the third column for sample 866) increased approximately by 20%, while for the terms corresponding to the tunneling magnetoresistance we had to increase these values approximately by a factor of 2.7. As a result, the resistance peak near the zero field in Fig. 7 is described by the term corresponding to the anisotropic magnetoresistance in the lead parts of the film, while the sharp increase following by the same sharp decrease near 200 Oe is described by the contribution from the tunneling magnetoresistance of the bicrystal junction.

Generally speaking, the increase in uniaxial anisotropy with decreasing temperature in LSMO films grown on NGO substrates is not an obvious fact. There are contradictory data in the literature on that score, and they were obtained indirectly [10, 42]. Our results can also be considered as an indirect argument for the increase in uniaxial anisotropy with decreasing temperature. At the same time, more direct measurements of the temperature dependence of the uniaxial anisotropy are required.

Several words should be said about the possibilities of increasing the tunneling magnetoresistance effect in LSMO films in which a significant spin polarization  $P$  is reached already at room temperature. It follows from our analysis of Eq. (3) that an increase in  $R_{sp}/R_0$  will lead to a growth of the effect. Of course, it is better to increase this ratio through a decrease in the resistance of the lead areas of the film. In addition, it is desirable to create a bicrystal film with aligned easy magnetization axes on both sides of the boundary while ensuring different anisotropy constants. In this case, apart from the maximal effect for an external magnetic field direction along the easy axes, the sharpest jumps will be ensured as the magnetoresistance both increases and decreases. These jumps will occur at external magnetic field strengths equal to  $H_{u1}$  and  $H_{u2}$ , respectively ( $H_{u1} < H_{u2}$ ).

## 5. CONCLUSIONS

Our measurement of the angular dependence of the magnetic field corresponding to FMR in bicrystal films and junctions revealed two ferromagnetically ordered spin subsystems with different directions of the easy magnetization axes. For bicrystal boundaries with rotation of the crystallographic axes of the basal planes of manganites around a direction perpendicular to the substrate plane (RB), the angles between the axes coincide with the crystallographic misorientation angles, while for bicrystal boundaries with rotation of

the basal planes around the bicrystal boundary line (TB), the magnetic misorientation is much smaller than the crystallographic one. In experiments with bicrystal boundaries based on LCMO films, the tunneling magnetoresistance reaches 160% at  $T = 4.2$  K. In LSMO junctions, the tunneling magnetoresistance is much lower and is observed against a background of the colossal and anisotropic magnetoresistances. The temperature dependences of the resistances for LCMO junctions exhibit an additional local peak due to the resistance of the boundary layer comparable to that of the films forming the bicrystal junction. In the case of LSMO bicrystal boundaries, no features are observed against a background of the resistance of the film itself. Both facts, the absence of a contribution and the sharp decrease in tunneling magnetoresistance, suggest that the width of the boundary (transition) layer in LSMO bicrystal films is much smaller than that in LCMO ones. At the same time, the presence of two peaks in the dependence of the magnetoresistance for LSMO bicrystal junctions suggests that the magnetic anisotropy in the boundary region is determined by the boundary and does not depend on temperature, while the uniaxial anisotropy in the film far from the boundary increases with decreasing temperature. The large characteristic resistance of the bicrystal boundary for LCMO restricts the observation of high-current spin-polarized carrier injection effects. One way to solve the problem may be the creation of a bicrystal film with aligned easy magnetization axes on both sides of the boundary but with different magnetic anisotropy constants.

## ACKNOWLEDGMENTS

We are grateful to V.A. Atsarkin, R. Gunnarson, P.E. Zil'berman, A.A. Klimov, K.I. Konstantinyan, I.M. Kotelyanskii, V.A. Luzanov, and S.A. Nikitov for a useful discussion of our results and help with our studies. This work was supported by programs of the Russian Academy of Sciences, the Ministry of Education and Science, (project no. 02.740.11.0795), a grant from the President of Russia for support of leading scientific schools (NSh-5423.2010.2), and the Russian Foundation for Basic Research (project nos. 11-02-01234a, 11-02-00349a).

## REFERENCES

1. I. Zutic, *Rev. Mod. Phys.* **76**, 323 (2004).
2. A. Kadigrobov, Z. Ivanov, T. Claeson, R. I. Shekhter, and M. Jonson, *Europhys. Lett.* **67**, 948 (2004).
3. M. Bowen, M. Bibes, A. Barthelemy, J.-P. Contour, A. Anane, Y. Lemaître, and A. Fert, *Appl. Phys. Lett.* **82**, 233 (2003).
4. J.-H. Park, E. Vescovo, H.-J. Kim, C. Kwon, R. Ramesh, and T. Venkatesan, *Nature (London)* **392**, 794 (1998).

5. R. von Helmholt, J. Wecker, B. Holzapfel, L. Schultz, and K. Samwer, *Phys. Rev. Lett.* **71**, 2331 (1993).
6. S. Jin, T. H. Tiefel, M. McCormack, R. A. Fastnacht, R. Ramesh, and L. H. Chen, *Science (Washington)* **264**, 413 (1994).
7. M. Ziese and S. P. Sena, *J. Phys.: Condens. Matter* **10**, 2727 (1998).
8. X. W. Li, A. Gupta, Gang Xiao, and G. Q. Gong, *Appl. Phys. Lett.* **71**, 1124 (1997).
9. J. O'Donnel, M. Onellion, and M. S. Rzchowski, *Phys. Rev. B: Condens. Matter* **55**, 5873 (1997).
10. K. Steenbeck and R. Hiergeist, *Appl. Phys. Lett.* **75**, 1778 (1999).
11. Z.-H. Wang, G. Cristiani, and H.-U. Habermeire, *Appl. Phys. Lett.* **82**, 3731 (2003).
12. M. Mathews, R. Jansen, G. Rijnders, J. C. Lodder, and D. H. A. Blank, *Phys. Rev. B: Condens. Matter* **80**, 064408 (2009).
13. H. Boschker, M. Mathews, E. P. Houwman, H. Nishikawa, A. Vailionis, G. Koster, G. Rijnders, and D. H. A. Blank, *Phys. Rev. B: Condens. Matter* **79**, 214425 (2009).
14. J. D. Fuhr, M. Granada, L. B. Steren, and B. Alasio, *J. Phys.: Condens. Matter* **22**, 146001 (2010).
15. Y. Basson, J. Hoffman, C. H. Ahn, and L. Klein, *Phys. Rev. B: Condens. Matter* **79**, 092406 (2009).
16. N. D. Mathur, G. Burnell, S. P. Isaac, T. J. Jackson, B.-S. Teo, J. L. MacManus-Driscoll, L. F. Cohen, J. E. Evetts, and M. G. Blamire, *Nature (London)* **387**, 266 (1997).
17. J. Klein, C. Höfener, S. Uhlenbruck, L. Alff, B. Büchner, and R. Gross, *Europhys. Lett.* **47**, 371 (1999).
18. R. Gunnarsson and M. Hanson, *Phys. Rev. B: Condens. Matter* **73**, 014435 (2006).
19. J. B. Philipp, C. Höfener, S. Thienhaus, J. Klein, L. Alff, and R. Gross, *Phys. Rev. B: Condens. Matter* **62**, R9248 (2000).
20. S. P. Isaac, N. D. Mathur, J. T. Evetts, and M. G. Blamire, *Appl. Phys. Lett.* **72**, 2039 (1996).
21. Y. Y. Divin, U. Poppe, C. L. Jia, P. M. Shadrin, and K. Urban, *Physica C (Amsterdam)* **372–376**, 115 (2002).
22. I. V. Borisenko and G. A. Ovsyannikov, *Phys. Solid State* **51** (2), 309 (2009).
23. G. Alejandro, L. B. Steren, H. Pastoriza, D. Vega, M. Granada, J. C. R. Sánchez, M. Sirena, and B. Alascio, *J. Phys.: Condens. Matter* **22**, 346007 (2010).
24. V. V. Demidov, I. V. Borisenko, A. A. Klimov, G. A. Ovsyannikov, A. M. Petrzhik, and S. A. Nikitov, *JETP* **112** (5), 825 (2011).
25. G. A. Ovsyannikov, A. M. Petrzhik, I. V. Borisenko, A. A. Klimov, Yu. A. Ignatov, V. V. Demidov, and S. A. Nikitov, *JETP* **108** (1), 48 (2009).
26. I. V. Borisenko, I. M. Kotelyanski, A. V. Shadrin, P. V. Komissinski, and G. A. Ovsyannikov, *IEEE Trans. Appl. Supercond.* **15**, 165 (2005).
27. B. A. Belyaev, A. V. Izotov, and S. Ya. Kiparisov, *JETP Lett.* **74** (4), 226 (2001).
28. A. E. Mefed and V. V. Demidov, *Instrum. Exp. Tech.* **51** (3), 418 (2008).
29. P. Dey, T. K. Nath, and A. Tarapher, *Appl. Phys. Lett.* **91**, 012511 (2007).
30. Yu. A. Izyumov and Yu. N. Skryabin, *Phys.—Usp.* **44** (2), 109 (2001).
31. Y. P. Lee, S. Y. Park, Y. H. Hyun, J. B. Kim, V. G. Prokhorov, V. A. Komashko, and V. L. Svetchnikov, *Phys. Rev. B: Condens. Matter* **73**, 224413 (2006).
32. R. Gunnarsson, M. Hanson, and C. Dობourdieu, *J. Appl. Phys.* **96**, 482 (2004); J. C. Slonczewski, *Phys. Rev. B: Condens. Matter* **39**, 6995 (1989).
33. G. Tatara and H. Fukuyama, *Phys. Rev. Lett.* **78**, 3773 (1997).
34. P. Lecoeur, P. L. Trouilloud, Gang Xiao, A. Gupta, G. Q. Gong, and X. W. Li, *J. Appl. Phys.* **82**, 3934 (1997).
35. N. D. Mathur, P. B. Littlewood, N. K. Todd, S. P. Isaac, B.-S. Teo, D.-J. Kang, E. J. Tarte, Z. H. Barber, J. E. Evetts, and M. G. Blamire, *J. Appl. Phys.* **86**, 6287 (1999).
36. J. Wolfman, A. M. Haghiri-Gosnet, B. Raveau, C. Vieu, E. Cambril, A. Cornette, and H. Launois, *J. Appl. Phys.* **89**, 6955 (2001).
37. S. V. Barabash and D. Stroud, *Appl. Phys. Lett.* **79**, 979 (2001).
38. Y. Bason, L. Klein, J.-B. Yau, X. Hong, and C. H. Ahn, *Appl. Phys. Lett.* **84**, 2593 (2004).
39. R. Gunnarsson, Z. G. Ivanov, C. Dობourdieu, and H. Russel, *Phys. Rev. B: Condens. Matter* **69**, 054413 (2004).
40. M. Julliere, *Phys. Lett. A* **54**, 225 (1975).
41. J. C. Slonczewski, *Phys. Rev. B: Condens. Matter* **39**, 6995 (1989).
42. K. Steenbeck, T. Habisreuther, C. Dობourdieu, and J. P. Sénateur, *Phys. Lett.* **80**, 3361 (2002).

*Translated by V. Astakhov*